ACS Energy LETTERS

http://pubs.acs.org/journal/aelccp

LETTER

Atomic-Layer-Deposition-Free Monolithic Perovskite/Silicon Tandem Solar Cell Reaching 29.91% Power Conversion on Industrial PERX/TOPCon-like Silicon Bottom Cells

Bor Li,[‖] Marlene Härtel,[‖] Amran Al-Ashouri, Maxim Simmonds, Isabella Taupitz, Lukas Kegelmann, Enrico Jarzembowski, Felix Frühauf, Eike Köhnen, Lars Korte, Fabian Fertig, Jörg Müller, and Steve Albrecht*

Cite This: *ACS Energy Lett.* 2024, 9, 4550−4556

Read Online

ACCESS | Metrics & More | Article Recommendations | Supporting Information

ABSTRACT: **Typically, the perovskite top-cell processes of monolithically integrated perovskite/silicon tandem solar cells (PSTSCs) include a slow and expensive atomic layer deposition (ALD) to grow a tin oxide (SnO_x) buffer layer protecting against sputter damage during the subsequent transparent top electrode deposition. We successfully replaced the ALD-SnO_x buffer layer with industry-compatible thermal evaporation of bathocuproine (BCP). By applying soft-sputter deposition of indium zinc oxide (IZO), we circumvent the increased risk of sputter damage when replacing ALD-SnO_x with organic BCP. In addition to technological advantages, this leads to a 20 mV gain in open-circuit voltage, similar charge extraction rates, and higher current densities due to less parasitic absorption, as confirmed by absolute and transient photoluminescence, current density−voltage, spectral responsivity, and transient surface photovoltage measurements. Integrating the BCP/IZO top contact into tandem solar cells enables a certified power conversion efficiency of 29.91% of our ALD-free PSTSC using industrial silicon bottom cells from Q CELLS' Q.ANTUM technology.**

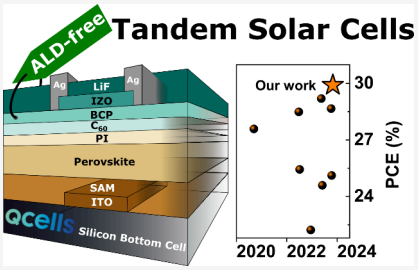

In the research field of highly efficient solar cells, perovskite/silicon tandem solar cells have gained considerable attention in recent years. Currently, crystalline silicon solar cells dominate the market, allowing for high-throughput and well-established fabrication that is generally not limited by the availability of critical raw materials.[1] This makes them highly attractive as bottom cells in tandem technology. While the current record monolithic perovskite/silicon tandem cells come with a silicon heterojunction (SHJ) bottom cell, other technologies, such as passivated emitter and rear contact/tunnel oxide passivated contact (PERx/TOPCon), are well established in the industry as well.[2] Compared with SHJ and TOPCon, the PERx architecture allows for a reduction in Ag consumption, as aluminum is used for the back contact. TOPCon also has the advantage of lower Ag consumption compared to SHJ, and additionally consumes less indium, with an overall lower consumption of critical materials compared to SHJ single-junction cells.[3] Regarding the choice of the bottom cell, the sustainability issue must be considered, especially when it comes to upscaling and industrialization.

Since only a few adaptions on silicon cells are needed to obtain industrially manufacturable bottom cells, it is crucial to work toward industrial-compatible processes for perovskite top cell fabrication. When sputter depositing the top transparent conductive oxide (TCO) electrode, a buffer layer is usually required to protect the subjacent perovskite absorber and its charge transport layers against sputter damage. ALD-deposited SnO_x, a dense metal oxide distinguished by its high chemical and thermal stability and low parasitic absorption, usually acts as a protective buffer layer for the subsequent sputter deposition of the TCO in lab-scale manufactured perovskite/silicon tandem solar cells.[4−6]

However, the utilization of an expensive ALD system and the increased process time hinder the commercialization and scale-up of industrial processes. One approach to address this

Received: June 3, 2024
Revised: August 7, 2024
Accepted: August 8, 2024
Published: August 26, 2024

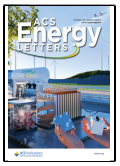

https://doi.org/10.1021/acsenergylett.4c01502
ACS Energy Lett. 2024, 9, 4550−4556

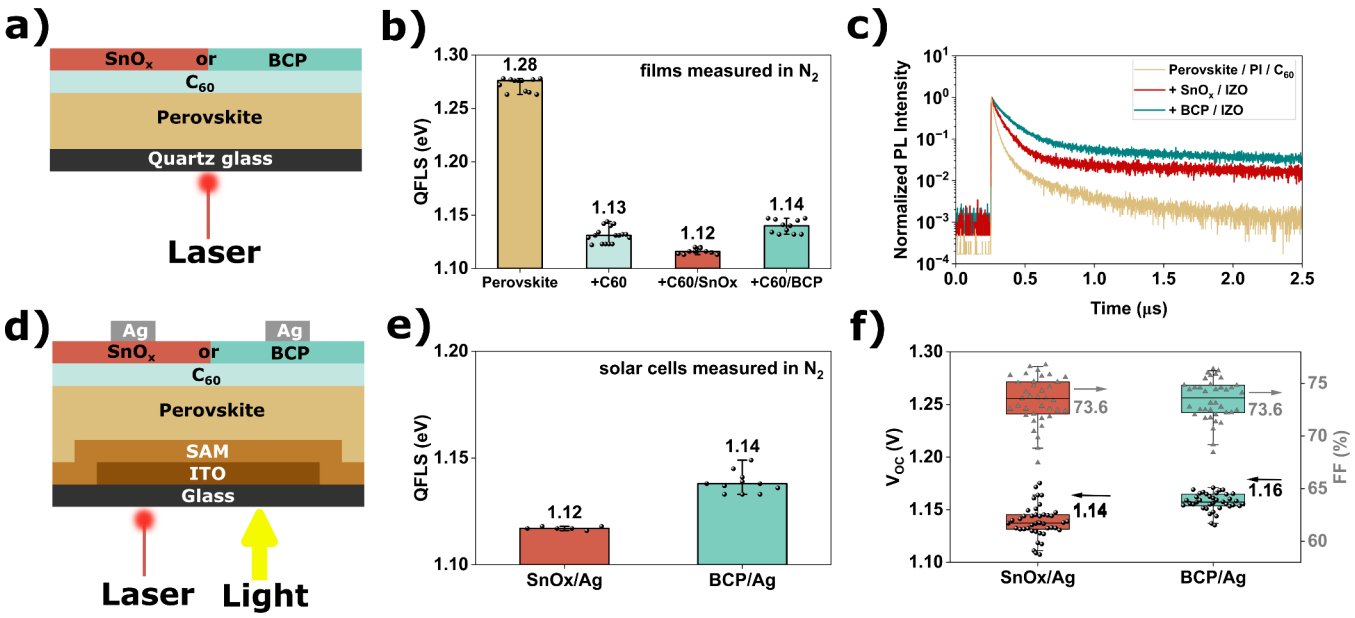

Figure 1. a) Schematic illustration of perovskite/C_{60} on top of quartz glass with either SnO_x (red) or BCP (cyan) excited by a laser for absolute photoluminescence measurement (abs. PL). b) Quasi-Fermi level splitting (QFLS) median values of bare perovskite on quartz and with C_{60} capped by SnO_x or BCP. Measured in nitrogen atmosphere. c) Normalized time-resolved photoluminescence (trPL) of perovskite/PI/C_{60} stacks without capping (yellow), and capped with either 10 nm SnO_x/40 nm IZO (red) or 8 nm BCP/40 nm IZO (cyan). d) Schematic illustration of an opaque perovskite single-junction solar cell with a p-i-n architecture for abs. PL and current−voltage (J−V) measurements with either SnO_x or BCP. e) QFLS of opaque perovskite single-junction solar cells with SnO_x or BCP. Measured in nitrogen atmosphere. f) Open-circuit voltage (V_{OC}) (left) and fill factor (FF) (right) of 36 opaque perovskite single-junction solar cells on six substrates, each with either SnO_x or BCP.

issue is to use spatial ALD, which has already been established for roll-to-roll processes.[7] Nevertheless, the precursor for ALD SnO_x deposition may degrade perovskite films and cells if the process is not delicately tailored to be soft on the perovskite.[8−11] In addition, the growth of the metal oxide on top of the fullerene (C_{60}) electron transport layer was shown to be nonoptimal, yielding complications such as subsurface and inhomogeneous growth.[12−15] Although methods have been proposed to improve the nucleation of SnO_x, such as ozone treatment of the C_{60} surface or implementation of PEIE as a seed layer,[12,13] incorporating these steps adds complexity to the solar cell fabrication process. Therefore, it is desirable to replace either the hazardous precursor material, namely tetrakis(dimethylamino)tin(IV) (TDMASn), or even the ALD process as a whole, ideally with subsequent thermal evaporation or other less expensive and scalable deposition methods after thermally evaporating C_{60}.

Here, we investigate the thermally evaporated bathocuproine (BCP), which is widely used as an electron transport layer (ETL) in combination with C_{60} in perovskite single-junctions and organic solar cells.[16−18] According to recent findings, BCP-based perovskite solar cells (PSC) have demonstrated greater intrinsic stability than SnO_x-based PSCs under substantial current stress because of the mitigation of copper electromigration throughout the entire cell stack.[19] In addition, it has been suggested that ALD-SnO_x triggers a perovskite phase transition in SnO_x-based PSCs under humid conditions, which may contribute to their decreased stability compared with BCP-based PSCs.[20] BCP has also been shown to have an encapsulation-like effect, protecting the subjacent layers against moisture and water.[21] However, replacing the protective SnO_x buffer layer with BCP introduces concerns regarding the vulnerability of the solar cell to sputter damage. A considerable fraction of the particles taking part in the sputter deposition process attain kinetic energies that could be harmful to the underlying layers. Although a certain level of kinetic energy of the sputtered particles is required for a uniform and dense TCO film growth, some particles can reach kinetic energies that are harmful to the layers underneath.[22,23] This can lead to defect-driven nonradiative recombination losses or impaired charge extraction.[4,24]

In that context, and similar to this work, Liu et al. compared the performances of perovskite devices based on BCP- and SnO_x-based ETLs.[25] Specifically, they investigated IZO sputter-deposition-induced damage and stress. They found that while BCP can, in fact, protect the underlying layers from sputter damage, it becomes damaged. Comparing sputter deposition of IZO onto thermally evaporated 8 nm BCP or 9 nm ALD SnO_x, they found that the 9 nm SnO_x-based device leads to a much better tandem performance, which correlates to the resilience of SnO_x against bombarding particles with high kinetic energies. In turn, Wahl et al. argued that they indeed did not see the need for an ALD SnO_x buffer layer, presenting their results on ALD SnO_x-free semitransparent perovskite solar cells.[26] They investigated the sputter damage resilience of solution-processed versus thermally evaporated ETL layers, including PCBM, C_{60}, and BCP. They found that a fully evaporated ETL stack was more resilient than a solution-processed stack. However, the solution-processed stack promotes curing sputter damage-induced defects, improving the performance after a few seconds at the 90 °C curing step, a method that has been presented in a different publication.[27] Notably, it has also been previously shown that in combination with Ag, BCP can be deployed as a buffer layer for sputtering processes.[28]

https://doi.org/10.1021/acsenergylett.4c01502
ACS Energy Lett. 2024, 9, 4550−4556

Based on our previous results,[29] this work focuses on the suitability of thermally evaporated BCP as a replacement for ALD-deposited SnO_x in perovskite/silicon tandem solar cells. Given the inherent sensitivity of the BCP material to the bombardment of particles with high kinetic energy, as opposed to the comparatively more robust SnO_x due to its higher bond energies,[25] we utilized an optimized low-damage RF sputter deposition of the top TCO, namely indium zinc oxide (IZO), to avert sputter-induced damage.

A comparative analysis between SnO_x and BCP involved integrating both films into perovskite single-junction (SJ) solar cells and stacks. Both the opaque and semitransparent SJ designs were systematically examined for their electrical and optical properties. Solar cell results show an increase in V_{OC} by 20 mV when using BCP compared to SnO_x, which was investigated in detail by employing spectroscopic measurement techniques, such as absolute and transient photoluminescence (absPL, trPL) and external quantum efficiency (EQE).

Eventually, we realized monolithic perovskite/silicon tandem solar cells utilizing industrial silicon bottom cells based on Q CELLS' Q.ANTUM technology. The improvements by replacing SnO_x with BCP could be transferred to tandems, leading to both optical and electrical benefits for the tandem solar cell, such as a 0.4 mA/cm^2 photocurrent gain in the top perovskite cell and a 10 mV gain in the overall V_{OC}. Therefore, the optimized BCP/IZO top layer achieved one of the highest certified efficiencies of 29.91% for perovskite/silicon tandem solar cells based on non-SHJ bottom cells.

To begin with, a comparative study of bare perovskite films[5,29] comprising $FA_{0.78}Cs_{0.22}Pb(I_{0.85}Br_{0.15})_3$ with 5 mol % MACl and $PbCl_2$ additives on quartz glass and in single-junction solar cell devices incorporating either ALD SnO_x or evaporated BCP was conducted to identify the advantages and benefits of each layer. Absolute photoluminescence was measured on quartz/perovskite/(C_{60})/(SnO_x or BCP) (see Figure 1a) to systematically investigate the photoluminescence quantum yield (PLQY) and nonradiative recombination losses induced by the additional interfaces. Figure 1b shows the quasi-Fermi level splitting (QFLS) values obtained from these measurements. The pristine perovskite film spin-coated on quartz glass demonstrated the highest QFLS value of approximately 1.27 eV, while the addition of thermally evaporated 18 nm C_{60} resulted in a decrease in QFLS to 1.13 eV. In previous studies, this was ascribed to increased interface defect densities and nonideal energy level alignment.[30−33] The introduction of ALD-deposited 10 nm SnO_x onto the perovskite/C_{60} sample resulted in a further reduction in the QFLS to 1.12 eV. In contrast, the employment of evaporated 8 nm BCP atop the C_{60} leads to a slightly higher QFLS of 1.14 eV. These results imply additional nonradiative recombination due to the SnO_x layer, which can be attributed to either the formation of defects and/or structural deterioration of the perovskite interface due to the ALD process,[8,9,11] or to the subsurface growth of SnO_x on C_{60}.[9,12] The slightly higher QFLS when BCP is placed on top of C_{60} may indicate a decrease in nonradiative recombination, which could be attributed to reduced interface damage and/or less recombination at the perovskite/C_{60} interface or within the C_{60}, as it is not fully selective.[34−36] Figure S1 in the Supporting Information shows scanning electron microscopy images of these films, illustrating the growth of both BCP and SnO_x on C_{60}. The images reveal a distinct difference in the growth morphology between SnO_x and BCP, with SnO_x exhibiting island growth. This results in a nonclosed SnO_x film on C_{60} with a thickness of 10 nm and a closed film with a thickness of 20 nm (see Figure S2a and b). Electrically, this seems to have no noticeable impact, as the FF and Voc of the devices built with both SnO_x thicknesses show no clear differences (see Figure S2c).When examining the QFLS values of complete opaque single-junction solar cell devices with a stack of ITO/Me-4PACz/perovskite/C_{60}/BCP or SnO_x/Ag (see Figure 1e), it becomes evident that there are similar discrepancies compared with films on quartz glass. Devices featuring SnO_x exhibited a QFLS value of approximately 1.12 eV, whereas those with BCP displayed a value of roughly 1.14 eV. Subsequently, we show the improved electronic properties associated with the utilization of BCP in comparison with SnO_x through a qualitative assessment of the illuminated $J-V$ characteristics, such as V_{OC} and FF. As shown in Figure 1f, opaque perovskite single-junction devices with SnO_x exhibited a V_{OC} of 1.14 V, which was lower than for the devices with BCP with a V_{OC} of 1.16 V. This 20 mV difference agrees with the QFLS values. Although it is possible that devices with SnO_x could reach a V_{OC} of 1.16 V, the median V_{OC} of devices with BCP was approximately 20 mV higher than that of devices with SnO_x across 36 single-junction solar cells on six substrates, each cell with an active area of 0.16 cm^2. These results align with the lower nonradiative recombination and charge accumulation at the C_{60}/BCP interface[19,34] than at the C_{60}/SnO_x interface, which is corroborated by the equal improvements in QFLS and V_{OC}.

An identical average fill factor of 73.6% for solar cells utilizing either SnOx or BCP is shown in Figure 1f. To further elucidate the FF and V_{OC} changes between the SnO_x and BCP buffer layers, we employed time-resolved PL (trPL) (Figure 1c) measurements to study the charge-carrier extraction efficiency and recombination behavior in the electron-selective layers. The perovskite samples underwent a surface treatment with piperazinium iodide (PI),[5,35,37] followed by encapsulation to minimize nonradiative recombination at the perovskite/C60 interface and to protect against external influences in ambient air. The PL transients of perovskite/PI/C_{60} films on quartz substrates that were either uncapped or capped with SnO_x/IZO or BCP/IZO were evaluated. These findings are presented in Figure 1c, revealing a noticeable difference in the PL decay times between the BCP and SnO_x samples. When utilizing BCP, the initial decay of the PL is considerably slower than that of SnO_x, indicating a reduction in nonradiative pathways and/or a reduction in the charge extraction efficiency. Additional trSPV measurements were conducted to further assess the extraction properties of these films and to rule out any alternative mechanisms causing PL quenching and faster PL decay.[38] The trSPV measurements, as shown in Figure S3, reveal a comparable carrier extraction behavior, which is indicated by a consistent signal rise during the initial 50 to 100 ns for both ETL configurations, perovskite/PI/C_{60}/SnO_x/IZO and perovskite//PI/C_{60}/BCP/IZO. Given the findings from the full solar cell electrical measurements, which demonstrate similar fill factors and charge extraction efficiencies based on the trSPV measurements, it can be inferred that the slower PL decay with BCP is primarily due to the reduction in nonradiative recombination pathways.

Semitransparent Single-Junction and Tandem Solar Cells. To further improve the PCE, the perovskite was post-treated with PI. We demonstrate its impact on opaque and semitransparent perovskite single-junction solar cell config-

https://doi.org/10.1021/acsenergylett.4c01502
ACS Energy Lett. 2024, 9, 4550−4556

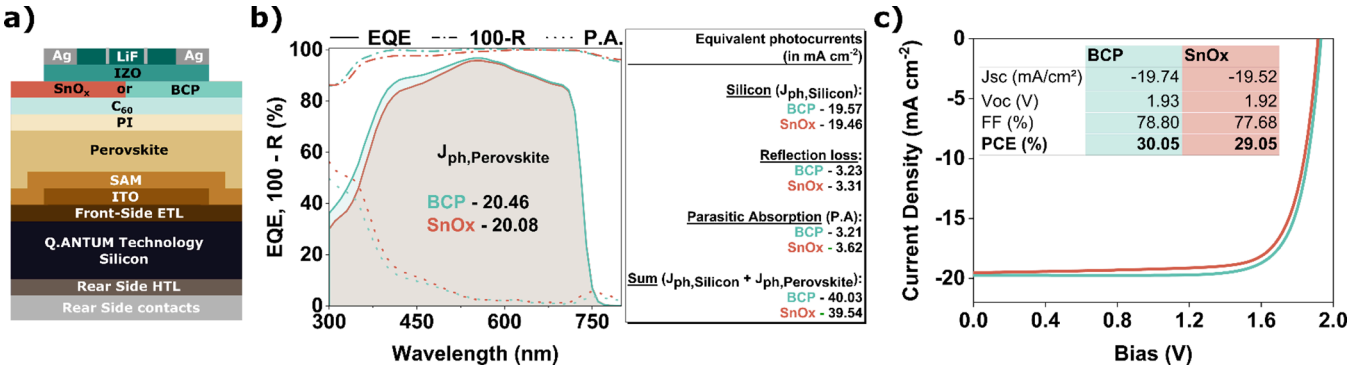

Figure 2. a) Schematic illustration of the perovskite/silicon tandem solar cell stack. b) Optical performance of a perovskite/silicon tandem solar cell. External quantum efficiency (EQE) spectra of the perovskite and silicon subcells in the tandem solar cell with either SnO_x (red) or BCP (cyan) layers, with the integrated photocurrent (J_{ph}) of the respective subcell shown in the inset text. Note that the EQE of the Silicon is not shown due to compliance. The optical reflectance of the device is represented by 100 − R (dash-dotted line) and the parasitic absorption (P.A) by 100 − R − EQE (dotted line). The equivalent photocurrents of the reflection loss, parasitic absorption, and the sum of both subcell are given in mA cm^{-2}. c) Current−voltage (J−V) characteristics of the champion perovskite/silicon tandem solar cell with the performance parameters in the inset table measured from V_{OC} to J_{SC}.

urations (Figure S4). For semitransparent cells, IZO was deposited as the transparent front electrode through a soft-sputtering process with reduced sputter power.[4] The electrical parameters are shown in Figure S4b. Opaque and semitransparent perovskite single-junction solar cells incorporating PI can achieve a significant V_{OC} enhancement of over 100 mV. The median V_{OC} of the devices with BCP reached a value of 1.27 V, which was on par with the QFLS of bare perovskite on quartz glass. In contrast, the cells treated with SnO_x still exhibited a reduced V_{OC} of 1.25 V, suggesting that the PI treatment did not influence the 20 mV V_{OC} difference between BCP and SnO_x. In addition, the stability of opaque and semitransparent devices was assessed by monitoring their shelf life for several months and conducting overnight MPP tracking, as shown in Figure S5.

Next, we integrated the semitransparent perovskite cell as the top cell into a *monolithic perovskite/silicon tandem solar cell* configuration using a silicon bottom cell fabricated using Q CELLS' Q.ANTUM technology (Figure 2a). The perovskite top cell was fabricated in the same manner as semitransparent perovskite single-junction solar cells. The optical and electrical characteristics of tandem solar cells with either SnO_x or BCP are shown in Figure 2. The external quantum efficiencies (EQE) of the tandem solar cells with BCP and SnO_x are shown in Figure 2b. The tandem cell with BCP reaches photogenerated current densities (J_{ph}) of 20.46 and 19.57 mA cm^{-2} for the perovskite and silicon cell, respectively, resulting in a total photocurrent of 40.03 mA cm^{-2}. In contrast, the tandem solar cell with SnO_x shows J_{ph} values of 20.08 and 19.46 mA cm^{-2} for the perovskite top cell and silicon bottom cell, respectively, with a total photocurrent of 39.54 mA cm^{-2}. Comparing the perovskite top cells of both configurations, the improvement in photocurrent density with BCP amounts to 0.38 mA cm^{-2}. The tandem solar cell with BCP exhibits reduced reflection losses equivalent to 0.08 mA cm^{-2} with the AM1.5 g spectrum, and parasitic absorption is reduced by 0.41 mA cm^{-2}, mostly at wavelengths of 300 to 600 nm. This correlates well with the lower absorption of BCP in that spectral range compared to SnO_x, as illustrated by the optical spectra of the films shown in Figure S6 in the SI. For the bottom cell, no impact from parasitic absorption of either of the layers in this range is expected to affect the charge carrier generation. This is reflected in the negligible difference in the respective bottom cell's integrated current density of 19.57 mA cm^{-2} for BCP- and 19.46 mA cm^{-2} for SnO_x-based tandem devices. The higher photocurrent in the top cell of the BCP-based tandem solar cell leads to a higher top-to-bottom cell current density mismatch of 0.89 mA cm^{-2} compared to devices with SnO_x, which are mismatched by 0.62 mA cm^{-2}. Hence, the increase in the overall tandem J_{SC} was limited by the silicon bottom cell, which resulted in a relatively minor improvement. Tandem solar cells with BCP thus present a greater disparity in the subcell current density mismatch than those with SnO_x, suggesting an even higher efficiency potential for this approach when optimizing both subcell currents.

We assume that this higher photocurrent density mismatch mainly contributes to the slightly higher FF in the J−V measurement,[39] as shown in Figure 2c. The tandem solar cell with SnO_x yields a V_{OC} of 1.92 V, a short-circuit current density of 19.52 mA cm^{-2}, and a FF of 77.68%, resulting in a PCE of 29.05% (certified 29.11%). The champion device with BCP outperformed the SnO_x-based cell, exhibiting a V_{OC} of 1.93 V, J_{SC} of 19.74 mA cm^{-2}, and FF of 78.8%, resulting in a higher PCE of 30.05% (certified 29.91%). The higher V_{OC} of perovskite single-junction cells with a BCP also translates into tandem devices. The overall increase in J_{SC}, FF, and V_{OC} with BCP led to an absolute PCE increase of 0.8% compared to the tandem device with SnO_x. To demonstrate the reproducibility of these results, Figure S7 shows the J_{SC}, V_{OC}, FF, and PCE results for several tandem cells with and without PI, as well as with BCP or SnO_x. Statistically, the tandem devices with BCP yielded higher V_{OC} and FF values, emphasizing the benefit compared to cells with ALD-SnO_x. The certificates for a tandem device with ALD-SnO_x (certified by the National Renewable Energy Laboratory (NREL)) and evaporated BCP (certified by the European Solar Test Installation (ESTI)) are shown in Figures S8 and S9, respectively.

We have created a J−V performance parameter compilation of previously published monolithic two-terminal perovskite/silicon tandem solar cells (Figure S10), showing that this is one of the highest reported efficiencies for a tandem solar cell featuring a type of silicon bottom cell, which is widely used in today's industry.[38−43]

https://doi.org/10.1021/acsenergylett.4c01502
ACS Energy Lett. 2024, 9, 4550−4556

In summary, this work addresses a key challenge of the conventional perovskite top cell process by replacing the slow and costly ALD process of the SnO_x buffer layer with a more industry-compatible thermal evaporation of BCP. Furthermore, the risk of sputter damage to the organic BCP, which may lack sufficient protection properties, was alleviated through the deliberate choice of a soft-sputter deposition process during the subsequent deposition of the transparent top electrode made of IZO. This technological optimization in device manufacturing addresses potential bottlenecks in industrial production lines by simplifying and accelerating the process flow and avoiding hazardous materials but also brings tangible solar cell performance benefits. The optimized BCP/IZO top stack resulted in a 20 mV increase in the open-circuit voltage for semitransparent single-junction devices, which is reflected in a higher QFLS measured by absolute PL, hinting at lower nonradiative recombination losses. Based on the trPL measurements, the PL decay with BCP exhibits a slower rate, which is indicative of a lower rate of nonradiative recombination. This is consistent with the findings of a similar FF in the complete device and charge extraction rates comparable to those of SnO_x in the trSPV measurements. The similar nonradiative recombination behavior of perovskite/C_{60}/BCP compared to perovskite/C_{60} stacks without an additional capping layer in absolute photoluminescence (PL) measurements suggests that the properties of the perovskite/C_{60} interface remain unchanged. Furthermore, electron microscopy images revealed that unlike BCP, SnO_x displays island-like growth, leading to a nonclosed film on C_{60} with a thickness below 20 nm. Interestingly, while the SnO_x film becomes closed at 20 nm thickness, this seems to have no noticeable impact electrically, as the FF and V_{OC} of the devices built with both SnO_x thicknesses show no clear differences, as shown in Figure S2 in the SI.

Regarding the stability of single-junction devices based on either BCP or 10 nm SnO_x, we could not find any advantage in using one layer over the other in the device. Opaque cells exhibited similar degradation in both cases concerning shelf life measurements over several months, and overnight MPP tracking of opaque and semitransparent devices showed almost identical behavior after a burn-in period, with continuous stability over several hours (see Figure S5).

When the BCP/IZO top stack was integrated into tandem devices using silicon bottom cells fabricated using Q CELLS' Q.ANTUM technology, the measured J_{ph} of the perovskite top cell was 0.38 mA cm^{-2} higher for the BCP-based devices, leading to a higher total current density. This increase resulted from the reduced parasitic absorption in the top cell compared with the SnO_x-based tandem devices. The successful integration of the optimized BCP/IZO top stack into tandem solar cells resulted in the highest certified steady-state efficiency of 29.91% for an ALD SnO_x buffer-free perovskite tandem device using industrial silicon bottom cells. This achievement underlines the feasibility of ALD-free monolithic two-terminal perovskite/silicon tandem solar cells and paves the way for their wide application in the photovoltaics industry.

■ ASSOCIATED CONTENT

Supporting Information

The Supporting Information is available free of charge at https://pubs.acs.org/doi/10.1021/acsenergylett.4c01502.

Materials and experimental details for perovskite single-junction and tandem solar cell fabrication, device characterization description, figures as described in the text, plots of $J-V$ parameters of the best cells from published two-terminal perovskite/silicon tandem solar cells, and tandem solar cell certification (PDF)

■ AUTHOR INFORMATION

Corresponding Author

Steve Albrecht − *Department Perovskite Tandem Solar Cells, Helmholtz-Zentrum Berlin für Materialien und Energie GmbH, 12489 Berlin, Germany;* orcid.org/0000-0001-9962-9535; Email: steve.albrecht@helmholtz-berlin.de

Authors

Bor Li − *Department Perovskite Tandem Solar Cells, Helmholtz-Zentrum Berlin für Materialien und Energie GmbH, 12489 Berlin, Germany;* orcid.org/0000-0003-3895-0792

Marlene Härtel − *Department Perovskite Tandem Solar Cells, Helmholtz-Zentrum Berlin für Materialien und Energie GmbH, 12489 Berlin, Germany;* orcid.org/0000-0002-1251-9745

Amran Al-Ashouri − *Department Perovskite Tandem Solar Cells, Helmholtz-Zentrum Berlin für Materialien und Energie GmbH, 12489 Berlin, Germany*

Maxim Simmonds − *Department Perovskite Tandem Solar Cells, Helmholtz-Zentrum Berlin für Materialien und Energie GmbH, 12489 Berlin, Germany; Department Solution Processing of Hybrid Materials and Devices, Helmholtz-Zentrum Berlin für Materialien und Energie GmbH, 12489 Berlin, Germany*

Isabella Taupitz − *Department Perovskite Tandem Solar Cells, Helmholtz-Zentrum Berlin für Materialien und Energie GmbH, 12489 Berlin, Germany*

[⊥]**Lukas Kegelmann** − *Hanwha Q CELLS GmbH, 06766 Bitterfeld-Wolfen, Germany*

[⊥]**Enrico Jarzembowski** − *Hanwha Q CELLS GmbH, 06766 Bitterfeld-Wolfen, Germany*

[⊥]**Felix Frühauf** − *Hanwha Q CELLS GmbH, 06766 Bitterfeld-Wolfen, Germany*

Eike Köhnen − *Department Perovskite Tandem Solar Cells, Helmholtz-Zentrum Berlin für Materialien und Energie GmbH, 12489 Berlin, Germany;* orcid.org/0000-0002-3637-4907

Lars Korte − *Department Perovskite Tandem Solar Cells, Helmholtz-Zentrum Berlin für Materialien und Energie GmbH, 12489 Berlin, Germany;* orcid.org/0000-0002-9207-9048

[#]**Fabian Fertig** − *Hanwha Q CELLS GmbH, 06766 Bitterfeld-Wolfen, Germany*

●**Jörg Müller** − *Hanwha Q CELLS GmbH, 06766 Bitterfeld-Wolfen, Germany*

Complete contact information is available at: https://pubs.acs.org/10.1021/acsenergylett.4c01502

Author Contributions

[‖]B.L. and M.H. contributed equally.

Notes

The authors declare no competing financial interest.

[⊥]L.K., E.J., and F.Fr. are Senior R&D Scientists at Hanwha Q CELLS GmbH.

https://doi.org/10.1021/acsenergylett.4c01502
ACS Energy Lett. 2024, 9, 4550−4556

[#]F.Fe. is the Head of the Department R&D Advanced Cells of Hanwha Q CELLS GmbH.
[●]J.M. is Head of Global R&D of Hanwha Q CELLS GmbH.

■ ACKNOWLEDGMENTS

The authors wish to thank J. Beckedahl, C. Ferber, M., Wittig, T., Lußky, and H. Heinz for technical support in the HySPRINT lab and the entire R&D team at Hanwha Q CELLS GmbH. We also thank F. Ruske and A. Miaskiewicz for SEM technical support. Funding was provided by the German Federal Ministry for Economic Affairs and Climate Action (BMWK) within the project PeroQ (grant no. 03EE118A) and by the Federal Ministry for Education and Research (BMBF) within the project PEROWIN (grant no. 03SF0631). Further funding is acknowledged by the HyperCells Graduate School. This work was supported by the Helmholtz Association within the EU-Partnering project TAPAS (Tandem Perovskite and Silicon Solar Cells Advanced Optoelectrical Characterization, Modelling and Stability) and the HySPRINT Helmholtz Innovation Lab. Hanwha Q CELLS GmbH prepared and supplied the silicon bottom-cells used in this manuscript.

■ REFERENCES

(1) Ghosh, D. K.; Bose, S.; Das, G.; Acharyya, S.; Nandi, A.; Mukhopadhyay, S.; Sengupta, A. Fundamentals, Present Status and Future Perspective of TOPCon Solar Cells: A Comprehensive Review. *Surfaces and Interfaces* **2022**, *30*, No. 101917.
(2) García Cerrillo, J.; Distler, A.; Matteocci, F.; Forberich, K.; Wagner, M.; Basu, R.; Castriotta, L. A.; Jafarzadeh, F.; Brunetti, F.; Yang, F.; Li, N.; Corpus-Mendoza, A. N.; Di Carlo, A.; Brabec, C. J.; Egelhaaf, H. J. Matching the Photocurrent of 2-Terminal Mechanically-Stacked Perovskite/Organic Tandem Solar Modules by Varying the Cell Width. *Solar RRL* **2023**, *8* (3), No. 2300767.
(3) Wang, L.; Zhang, Y.; Kim, M.; Wright, M.; Underwood, R.; Bonilla, R. S.; Hallam, B. Sustainability Evaluations on Material Consumption for Terawatt-Scale Manufacturing of Silicon-Based Tandem Solar Cells. *Progress in Photovoltaics: Research and Applications* **2023**, *31* (12), 1442−1454.
(4) Härtel, M.; Li, B.; Mariotti, S.; Wagner, P.; Ruske, F.; Albrecht, S.; Szyszka, B. Reducing Sputter Damage-Induced Recombination Losses during Deposition of the Transparent Front-Electrode for Monolithic Perovskite/Silicon Tandem Solar Cells. *Sol. Energy Mater. Sol. Cells* **2023**, *252*, No. 112180.
(5) Mariotti, S.; Köhnen, E.; Scheler, F.; Sveinbjörnsson, K.; Zimmermann, L.; Piot, M.; Yang, F.; Li, B.; Warby, J.; Musiienko, A.; Menzel, D.; Lang, F.; Keßler, S.; Levine, I.; Mantione, D.; Al-Ashouri, A.; Härtel, M. S.; Xu, K.; Cruz, A.; Kurpiers, J.; Wagner, P.; Köbler, H.; Li, J.; Magomedov, A.; Mecerreyes, D.; Unger, E.; Abate, A.; Stolterfoht, M.; Stannowski, B.; Schlatmann, R.; Korte, L.; Albrecht, S. Interface Engineering for High-Performance, Triple-Halide Perovskite-Silicon Tandem Solar Cells. *Science* **2023**, *381* (6653), 63−69.
(6) Al-Ashouri, A.; Köhnen, E.; Li, B.; Magomedov, A.; Hempel, H.; Caprioglio, P.; Márquez, J. A.; Vilches, A. B. M.; Kasparavicius, E.; Smith, J. A.; Phung, N.; Menzel, D.; Grischek, M.; Kegelmann, L.; Skroblin, D.; Gollwitzer, C.; Malinauskas, T.; Jošt, M.; Matič, G.; Rech, B.; Schlatmann, R.; Topič, M.; Korte, L.; Abate, A.; Stannowski, B.; Neher, D.; Stolterfoht, M.; Unold, T.; Getautis, V.; Albrecht, S. Monolithic Perovskite/Silicon Tandem Solar Cell with > 29% Efficiency by Enhanced Hole Extraction. *Science (1979)* **2020**, *370* (6522), 1300−1309.
(7) Schiefer, S. *Durchkontaktierte Organische Solarzellen*. Fraunhofer Verlag: 2014. https://doi.org/10.24406/publica-fhg-280183.
(8) Palmstrom, A. F.; Raiford, J. A.; Prasanna, R.; Bush, K. A.; Sponseller, M.; Cheacharoen, R.; Minichetti, M. C.; Bergsman, D. S.; Leijtens, T.; Wang, H. P.; Bulović, V.; McGehee, M. D.; Bent, S. F. Interfacial Effects of Tin Oxide Atomic Layer Deposition in Metal Halide Perovskite Photovoltaics. *Adv. Energy Mater.* **2018**, *8* (23), No. 1800591.
(9) Hultqvist, A.; Jacobsson, T. J.; Svanström, S.; Edoff, M.; Cappel, U. B.; Rensmo, H.; Johansson, E. M. J.; Boschloo, G.; Törndahl, T. SnOxAtomic Layer Deposition on Bare Perovskite - An Investigation of Initial Growth Dynamics, Interface Chemistry, and Solar Cell Performance. *ACS Appl. Energy Mater.* **2021**, *4* (1), 510−522.
(10) Mallik, N.; Hajhemati, J.; Frégnaux, M.; Coutancier, D.; Toby, A.; Zhang, S.-T.; Hartmann, C.; Hüsam, E.; Saleh, A.; Vincent, T.; Fournier, O.; Wilks, R. G.; Aureau, D.; Félix, R.; Schneider, N.; Bär, M.; Schulz, P. Interface Defect Formation for Atomic Layer Deposition of SnO2 on Metal Halide Perovskites. *Nano Energy* **2024**, *126*, No. 109582.
(11) Bracesco, A. E. A.; Jansen, J. W. P.; Xue, H.; Zardetto, V.; Brocks, G.; Kessels, W. M. M.; Tao, S.; Creatore, M. In Situ IR Spectroscopy Studies of Atomic Layer-Deposited SnO2 on Formamidinium-Based Lead Halide Perovskite. *ACS Appl. Mater. Interfaces* **2023**, *15* (31), 38018−38028.
(12) Raiford, J. A.; Boyd, C. C.; Palmstrom, A. F.; Wolf, E. J.; Fearon, B. A.; Berry, J. J.; McGehee, M. D.; Bent, S. F. Enhanced Nucleation of Atomic Layer Deposited Contacts Improves Operational Stability of Perovskite Solar Cells in Air. *Adv. Energy Mater.* **2019**, *9* (47), 1−9.
(13) Johnson, S. A.; White, K. P.; Tong, J.; You, S.; Magomedov, A.; Larson, B. W.; Morales, D.; Bramante, R.; Dunphy, E.; Tirawat, R.; Perkins, C. L.; Werner, J.; Lahti, G.; Velez, C.; Toney, M. F.; Zhu, K.; McGehee, M. D.; Berry, J. J.; Palmstrom, A. F. Improving the Barrier Properties of Tin Oxide in Metal Halide Perovskite Solar Cells Using Ozone to Enhance Nucleation. *Joule* **2023**, *7* (12), 2873−2893.
(14) Xiong, Z.; Wu, L.; Zhou, X.; Yang, S.; Liu, Z.; Liu, W.; Zhao, J.; Li, W.; Yu, C.; Yao, K. Constructing Tin Oxides Interfacial Layer with Gradient Compositions for Efficient Perovskite/Silicon Tandem Solar Cells with Efficiency Exceeding 28%. *Small* **2024**, *20* (15), No. 2308024.
(15) Yu, B.; Tang, F.; Yang, Y.; Huang, J.; Wu, S.; Lu, F.; Duan, W.; Lambertz, A.; Ding, K.; Mai, Y. Impermeable Atomic Layer Deposition for Sputtering Buffer Layer in Efficient Semi-Transparent and Tandem Solar Cells via Activating Unreactive Substrate. *Adv. Mater.* **2023**, *35* (5), No. 2202447.
(16) Vogel, M.; Doka, S.; Breyer, C.; Lux-Steiner, M. C.; Fostiropoulos, K. On the Function of a Bathocuproine Buffer Layer in Organic Photovoltaic Cells. *Appl. Phys. Lett.* **2006**, *89* (16), No. 163501.
(17) Hao, X.; Wang, S.; Fu, W.; Sakurai, T.; Masuda, S.; Akimoto, K. Novel Cathode Buffer Layer of Ag-Doped Bathocuproine for Small Molecule Organic Solar Cell with Inverted Structure. *Org. Electron* **2014**, *15* (8), 1773−1779.
(18) Patil, B. R.; Ahmadpour, M.; Sherafatipour, G.; Qamar, T.; Fernández, A. F.; Zojer, K.; Rubahn, H. G.; Madsen, M. Area Dependent Behavior of Bathocuproine (BCP) as Cathode Interfacial Layers in Organic Photovoltaic Cells. *Sci. Rep* **2018**, *8* (1), 1−9.
(19) Lago, N.; Reddy, S. H.; Magliano, E.; Di Carlo, A.; Cester, A. Accelerated Constant Current Stress on Triple Cation Perovskite Solar Cells. *Sol. Energy Mater. Sol. Cells* **2023**, *262*, No. 112535.
(20) Zheng, Z.; Xue, Z.; Zhao, K.; Yang, Y.; Zhu, X.; Li, H.; Cheng, S.; Li, S.; Yan, N.; Wang, Z. Unveiling and Overcoming Instabilities in Perovskite Solar Cells Induced by Atomic-Layer-Deposition Tin Oxide. *Solar RRL* **2024**, *8* (8), No. 2301076.
(21) Chen, C.; Zhang, S.; Wu, S.; Zhang, W.; Zhu, H.; Xiong, Z.; Zhang, Y.; Chen, W. Effect of BCP Buffer Layer on Eliminating Charge Accumulation for High Performance of Inverted Perovskite Solar Cells. *RSC Adv.* **2017**, *7* (57), 35819−35826.
(22) Ellmer, K.; Welzel, T. Reactive Magnetron Sputtering of Transparent Conductive Oxide Thin Films: Role of Energetic Particle (Ion) Bombardment. *J. Mater. Res.* **2012**, *27* (5), 765−779.
(23) Aydin, E.; Altinkaya, C.; Smirnov, Y.; Yaqin, M. A.; Zanoni, K. P. S.; Paliwal, A.; Firdaus, Y.; Allen, T. G.; Anthopoulos, T. D.; Bolink, H. J.; Morales-Masis, M.; De Wolf, S. Sputtered Transparent

Electrodes for Optoelectronic Devices: Induced Damage and Mitigation Strategies. *Matter* **2021**, *4* (11), 3549−3584.
(24) Werner, J.; Dubuis, G.; Walter, A.; Löper, P.; Moon, S. J.; Nicolay, S.; Morales-Masis, M.; De Wolf, S.; Niesen, B.; Ballif, C. Sputtered Rear Electrode with Broadband Transparency for Perovskite Solar Cells. *Sol. Energy Mater. Sol. Cells* **2015**, *141*, 407−413.
(25) Liu, K.; Chen, B.; Yu, Z. J.; Wu, Y.; Huang, Z.; Jia, X.; Li, C.; Spronk, D.; Wang, Z.; Wang, Z.; Qu, S.; Holman, Z. C.; Huang, J. Reducing Sputter Induced Stress and Damage for Efficient Perovskite/Silicon Tandem Solar Cells. *J. Mater. Chem. A Mater.* **2022**, *10* (3), 1343−1349.
(26) Wahl, T.; Hanisch, J.; Becker, J. P.; Ahlswede, E. Influence of the Electron Transport Layer Coating Technique on Sputter Damage and Its Curing in Inverted Semi-Transparent Perovskite Solar Cells without Protective Buffer Layer. *Sol. Energy Mater. Sol. Cells* **2024**, *271*, No. 112825.
(27) Wahl, T.; Hanisch, J.; Meier, S.; Schultes, M.; Ahlswede, E. Sputtered Indium Zinc Oxide Rear Electrodes for Inverted Semi-transparent Perovskite Solar Cells without Using a Protective Buffer Layer. *Org. Electron* **2018**, *54*, 48−53.
(28) Ying, Z.; Yang, X.; Zheng, J.; Zhu, Y.; Xiu, J.; Chen, W.; Shou, C.; Sheng, J.; Zeng, Y.; Yan, B.; Pan, H.; Ye, J.; He, Z. Charge-Transfer Induced Multifunctional BCP:Ag Complexes for Semi-Transparent Perovskite Solar Cells with a Record Fill Factor of 80.1%. *J. Mater. Chem. A Mater.* **2021**, *9* (20), 12009−12018.
(29) Sveinbjörnsson, K.; Li, B.; Mariotti, S.; Jarzembowski, E.; Kegelmann, L.; Wirtz, A.; Frühauf, F.; Weihrauch, A.; Niemann, R.; Korte, L.; Fertig, F.; Müller, J. W.; Albrecht, S. Monolithic Perovskite/Silicon Tandem Solar Cell with 28.7% Efficiency Using Industrial Silicon Bottom Cells. *ACS Energy Lett.* **2022**, *7* (8), 2654−2656.
(30) Menzel, D.; Al-Ashouri, A.; Tejada, A.; Levine, I.; Guerra, J. A.; Rech, B.; Albrecht, S.; Korte, L. Field Effect Passivation in Perovskite Solar Cells by a LiF Interlayer. *Adv. Energy Mater.* **2022**, *12* (30), No. 2201109.
(31) Stolterfoht, M.; Caprioglio, P.; Wolff, C. M.; Márquez, J. A.; Nordmann, J.; Zhang, S.; Rothhardt, D.; Hörmann, U.; Amir, Y.; Redinger, A.; Kegelmann, L.; Zu, F.; Albrecht, S.; Koch, N.; Kirchartz, T.; Saliba, M.; Unold, T.; Neher, D. The Impact of Energy Alignment and Interfacial Recombination on the Internal and External Open-Circuit Voltage of Perovskite Solar Cells. *Energy Environ. Sci.* **2019**, *12* (9), 2778−2788.
(32) Warby, J.; Zu, F.; Zeiske, S.; Gutierrez-Partida, E.; Frohloff, L.; Kahmann, S.; Frohna, K.; Mosconi, E.; Radicchi, E.; Lang, F.; Shah, S.; Peña-Camargo, F.; Hempel, H.; Unold, T.; Koch, N.; Armin, A.; De Angelis, F.; Stranks, S. D.; Neher, D.; Stolterfoht, M. Understanding Performance Limiting Interfacial Recombination in Pin Perovskite Solar Cells. *Adv. Energy Mater.* **2022**, *12* (12), No. 2103567.
(33) Liu, J.; De Bastiani, M.; Aydin, E.; Harrison, G. T.; Gao, Y.; Pradhan, R. R.; Eswaran, M. K.; Mandal, M.; Yan, W.; Seitkhan, A.; Babics, M.; Subbiah, A. S.; Ugur, E.; Xu, F.; Xu, L.; Wang, M.; Ur Rehman, A.; Razzaq, A.; Kang, J.; Azmi, R.; Said, A. A.; Isikgor, F. H.; Allen, T. G.; Andrienko, D.; Schwingenschlögl, U.; Laquai, F.; De Wolf, S. Efficient and Stable Perovskite-Silicon Tandem Solar Cells through Contact Displacement by MgFx. *Science* **2022**, *377* (6603), 302−306.
(34) Wang, S.; Sakurai, T.; Kuroda, R.; Akimoto, K. Energy Level Alignment of C60/Ca Interface with Bathocuproine as an Interlayer Studied by Ultraviolet Photoelectron Spectroscopy. *Jpn. J. Appl. Phys.* **2012**, *51* (10S), No. 10NE32.
(35) Shibayama, N.; Kanda, H.; Kim, T. W.; Segawa, H.; Ito, S. Design of BCP Buffer Layer for Inverted Perovskite Solar Cells Using Ideal Factor. *APL Mater.* **2019**, *7* (3), No. 031117.
(36) Tomova, R.; Petrova, P.; Stoycheva-Topalova, R. Role of Bathocuproine as Hole-Blocking and Electron-Transporting Layer in Organic Light Emitting Devices. *Physica Status Solidi (C) Current Topics in Solid State Physics* **2010**, *7*, 992−995.
(37) Yang, F.; Tockhorn, P.; Musiienko, A.; Lang, F.; Menzel, D.; Macqueen, R.; Köhnen, E.; Xu, K.; Mariotti, S.; Mantione, D.; Merten, L.; Hinderhofer, A.; Li, B.; Wargulski, D. R.; Harvey, S. P.; Zhang, J.; Scheler, F.; Berwig, S.; Roß, M.; Thiesbrummel, J.; Al-Ashouri, A.; Brinkmann, K. O.; Riedl, T.; Schreiber, F.; Abou-Ras, D.; Snaith, H.; Neher, D.; Korte, L.; Stolterfoht, M.; Albrecht, S. Minimizing Interfacial Recombination in 1.8 EV Triple-Halide Perovskites for 27.5% Efficient All-Perovskite Tandems. *Adv. Mater.* **2024**, *36* (6), No. 2307743.
(38) Levine, I.; Al-Ashouri, A.; Musiienko, A.; Hempel, H.; Magomedov, A.; Drevilkauskaite, A.; Getautis, V.; Menzel, D.; Hinrichs, K.; Unold, T.; Albrecht, S.; Dittrich, T. Charge Transfer Rates and Electron Trapping at Buried Interfaces of Perovskite Solar Cells. *Joule* **2021**, *5* (11), 2915−2933.
(39) Köhnen, E.; Jošt, M.; Morales-Vilches, A. B.; Tockhorn, P.; Al-Ashouri, A.; Macco, B.; Kegelmann, L.; Korte, L.; Rech, B.; Schlatmann, R.; Stannowski, B.; Albrecht, S. Highly Efficient Monolithic Perovskite Silicon Tandem Solar Cells: Analyzing the Influence of Current Mismatch on Device Performance. *Sustain Energy Fuels* **2019**, *3* (8), 1995−2005.
(40) Ding, Z.; Liu, Z.; Xing, M.; Xue, X.; Yang, W.; Liu, W.; Liao, M.; Yang, Z.; Zeng, Y.; Ye, J. Highly Transparent Oxygen-Doped Poly-Si with In-Situ N2O Oxidant for Poly-Si Passivating Contacts in Perovskite/Silicon Tandem Solar Cells. *Solar RRL* **2024**, *8* (10), No. 2400134.
(41) Zheng, J.; Ying, Z.; Yang, Z.; Lin, Z.; Wei, H.; Chen, L.; Yang, X.; Zeng, Y.; Li, X.; Ye, J. Polycrystalline Silicon Tunnelling Recombination Layers for High-Efficiency Perovskite/Tunnel Oxide Passivating Contact Tandem Solar Cells. *Nat. Energy* **2023**, *8* (11), 1250−1261.
(42) Qiao, L.; Ye, T.; Wang, T.; Kong, W.; Sun, R.; Zhang, L.; Wang, P.; Ge, Z.; Peng, Y.; Zhang, X.; Xu, M.; Yan, X.; Yang, J.; Zhang, X.; Zeng, F.; Han, L.; Yang, X. Freezing Halide Segregation Under Intense Light for Photostable Perovskite/Silicon Tandem Solar Cells. *Adv. Energy Mater.* **2024**, *14* (7), No. 2302983.
(43) Jiang, S.; Ding, Z.; Li, X.; Zhang, L.; Ying, Z.; Yang, X.; Yang, Z.; Yang, W.; Zeng, Y.; Ye, J. Advancing Monolithic Perovskite/TOPCon Tandem Solar Cells by Customizing Industrial-Level Micro-Nano Structures. *Adv. Funct Mater.* **2024**, No. 2401900.

https://doi.org/10.1021/acsenergylett.4c01502
ACS Energy Lett. 2024, 9, 4550−4556